

End-to-End Dexterous Grasp Learning from Single-View Point Clouds via a Multi-Object Scene Dataset

Tao Geng, Dapeng Yang, *Senior*

Member, IEEE, Ziwei Liu, Le Zhang, Le Qi, WangYang Li, Yi Ren, *Member, IEEE*, Shan Luo, *Senior Member, IEEE*, Fenglei Ni

Abstract—Dexterous grasping in multi-object scene constitutes a fundamental challenge in robotic manipulation. Current mainstream grasping datasets predominantly focus on single-object scenarios and predefined grasp configurations, often neglecting environmental interference and the modeling of dexterous pre-grasp gesture, thereby limiting their generalizability in real-world applications. To address this, we propose DGS-Net, an end-to-end grasp prediction network capable of learning dense grasp configurations from single-view point clouds in multi-object scene. Furthermore, we propose a two-stage grasp data generation strategy that progresses from dense single-object grasp synthesis to dense scene-level grasp generation. Our dataset comprises 307 objects, 240 multi-object scenes, and over 350k validated grasps. By explicitly modeling grasp offsets and pre-grasp configurations, the dataset provides more robust and accurate supervision for dexterous grasp learning. Experimental results show that DGS-Net achieves grasp success rates of 88.63% in simulation and 78.98% on a real robotic platform, while exhibiting lower penetration with a mean penetration depth of 0.375 mm and penetration volume of 559.45 mm³, outperforming existing methods and demonstrating strong effectiveness and generalization capability. Our dataset is available at <https://github.com/4taotao8/DGS-Net>.

Index Terms—Robotic grasping in multi-object scene, grasping dataset, supervised deep learning

I. INTRODUCTION

GRASPING refers to the process of exerting forces and torques at a set of contact points to control an object’s motion in a desired manner [1]. As a core robotic capability, grasping is fundamental to higher-level tasks such as object manipulation, assembly, and physical interaction. However, identifying the optimal grasp among numerous candidates remains a challenging problem [2], [3].

Conventional approaches have mainly focused on parallel grippers and prior object knowledge [4]–[6]. By adopting simplified contact models, Coulomb friction, and rigid-body assumptions, they construct force-closure strategies [7] that perform well in simple, controlled environments. Yet, their low degrees of freedom and limited adaptability make them unsuitable for complex manipulation in unstructured settings. In contrast, multi-fingered dexterous hands emulate human morphology with enhanced kinematic redundancy, enabling diverse and precise grasping maneuvers—particularly beneficial for irregular objects, cluttered environments, and uncertain

poses [3], [8], [9]. Recent advances in computer vision and robotics have accelerated a shift toward data-driven dexterous grasping algorithms, aiming for more generalizable systems.

Nevertheless, current dexterous grasping systems still fall short of human-level dexterity [9]. Most prior work focuses on single, regularly-shaped objects [10]–[12], ignoring real-world complexities like occlusion and incomplete perception. Furthermore, many single-object approaches depend on pre-processing pipelines like SAM segmentation [13] and point cloud completion [14], while scene-level completion methods [15], struggle to balance real-time performance with reconstruction accuracy. These limitations constrain the robustness and generalization of dexterous grasping in practice.

Another key bottleneck is dataset acquisition. Collecting large-scale, high-quality grasp data in real settings is costly and labor-intensive [2]. Existing datasets primarily target parallel grippers [16], [17]. Recent efforts for dexterous hands [18], [19] still largely focus on single-object scenes and often omit pre-grasp configurations or environmental interactions. Pre-grasp configurations strongly affect grasp stability and success. The scarcity of multi-object, pre-grasp-aware dexterous datasets substantially limits the applicability and generalization of data-driven methods [20].

In summary, directly predicting complete high-DoF grasp configurations for dexterous hands from single-view, incomplete point clouds in multi-object scenes remains a challenging task. To address this, we propose an end-to-end grasp prediction network, DGS-Net. Furthermore, to support learning in complex scenes, we introduce a two-stage grasp data generation pipeline. Specifically, the main contributions of this work are as follows:

- An end-to-end grasp prediction network, DGS-Net: Based on the Point Transformer V3 [21] backbone, it can directly predict dexterous grasp configurations from single-view point clouds in multi-object scenes, demonstrating remarkable learning capability and generalization.
- A two-stage grasp data generation pipeline: We construct a dexterous grasping dataset from object-level to scene-level dense grasps, including 307 objects, 240 scenes, and 350k+ validated grasps, facilitating robust learning and generalization in real-world scenarios.
- More accurate and physically consistent grasp prediction: By explicitly modeling and predicting grasp offsets and pre-grasp configurations, our method effectively compensates for point cloud incompleteness and projection errors, enabling more precise hand-object alignment and significantly reducing penetration during grasp execution.

This work was supported in part by the National Natural Science Foundation of China under Grant T2388101, in part by the Huawei Industry-University Cooperation Project under Grant TC20250106029, and in part by the Pre-research Task (No. SKLRS202408B) of the State Key Laboratory of Robotics and Systems, Harbin Institute of Technology.

- **Robust real-world performance:** Our method achieves 80.39% success and 87.23% clearance on novel objects in real scenes, with 0.45s inference time, demonstrating high generalization and real-time capability.

II. RELATED WORKS

Grasping research can be categorized by end-effector type into parallel grippers and dexterous hands. For parallel grippers, grasp poses are typically represented by a 7D vector (3D translation, 3D rotation, and 1D gripper width), enabling extensive studies such as VGN [22], GraspNet-1Billion [16], and AnyGrasp [23]. In contrast, multi-fingered dexterous hands (e.g., DLR/HIT Hand II [24], Shadow Hand [25]) pose greater challenges due to their higher DoF and heterogeneous kinematics. Existing algorithms struggle to fully exploit their capabilities, motivating our focus on dexterous hand grasping.

Grasping methods are typically divided into analytical and data-driven approaches [2]. Analytical methods optimize grasp configurations to resist external forces and torques but rely on complete prior knowledge of object models and hand kinematics. As a result, they suffer from two major limitations: (i) exponentially large search spaces (despite dimensionality reduction efforts [6], [26]) and (ii) limited grasp diversity, making them unsuitable for novel objects.

Data-driven grasp planning methods employ deep or reinforcement learning to model the latent mapping from sensory data to multi-finger grasp configurations, thereby leveraging both perception and prior grasping experience for planning [1]. Most existing works rely on depth cameras for perception, which often results in incomplete point clouds. Some methods, such as DVGG [10], Multi-FinGAN [27], and Humt et al. [14], address this by segmenting and completing point clouds before predicting grasps, while FFHNet [11] directly predicts grasps from segmented single-view point clouds. However, these approaches focus on isolated objects and thus neglect inter-object relationships (e.g., occlusion, contact, or stacking), which may lead to collisions or incorrect grasp feasibility estimation. Scene-level grasp prediction has been explored by methods such as GraspNet-1Billion [16] and AnyGrasp [23] through end-to-end networks in cluttered environments. Nevertheless, most of these works are designed for parallel grippers. We argue that directly predicting high-DoF dexterous hand configurations in an end-to-end manner remains highly challenging. Among existing studies, HGC-Net [28] is most related to our work but restricts grasp poses to five predefined categories, thereby limiting the flexibility of dexterous hands. Very recently, DexGraspNet 2.0 [29] proposes a diffusion-based generative model conditioned on local geometric features for scene-level dexterous grasping. The method achieves state-of-the-art performance in multi-object grasping scenarios.

High-quality datasets are essential for advancing data-driven grasping algorithms, yet collecting real-world grasp data remains highly challenging. Most available datasets target parallel grippers, such as GraspNet-1Billion [16] and GraspClutter6D [17]. Some efforts, including DexYCB [30] and HO3D [31], provide human grasp demonstrations, while RealDex [32]

adapts human grasps for dexterous hands using a cVAE-based module. However, kinematic differences between human and robotic hands limit motion transferability. Simulation-based datasets such as DexGraspNet [19] and Dexonomy [33] generate large-scale grasps but remain restricted to single-object settings and lack consideration of inter-object occlusions in multi-object scenes. To address this limitation, DexGraspNet 2.0 [29] constructs an extremely large-scale synthetic dexterous grasping dataset for multi-object scenes using optimization-based grasp synthesis, covering thousands of scenes and hundreds of millions of grasp annotations. Although our dataset is smaller in scale, it achieves competitive grasp prediction accuracy and lower penetration during execution, owing to the explicit modeling of grasp offsets and pre-grasp configurations.

III. PROBLEM STATEMENT

Given a single-view, incomplete point cloud of a multi-object scene, our method employs a two-stage grasp prediction network that takes this point cloud as input and outputs grasp pose with corresponding joint configuration (including pre-grasp configuration) for multiple objects. The dexterous hand first moves to the predicted grasp pose using the pre-grasp configuration, and then executes the final grasp. In this work, we employ the DexHand Pro, a variant of the DLR/HIT Hand II [24], which features a modular design with five identical fingers, comprising 20 joints and 15 active degrees of freedom, as shown in Fig. 1(a).

Several key definitions are presented here:

Point Clouds: We denote the point cloud captured by the camera as $\mathcal{P} \in \mathbb{R}^{N \times 3}$, where N is the number of points.

Hand Grasps: The grasp configuration of the hand is represented as $G = (T, R, J_{\text{init}}, J_{\text{end}})$. Specifically, $T \in \mathbb{R}^3$ denotes the tool center point (TCP) of the dexterous hand, and $R \in \mathbb{R}^6$ represents the 6D rotation [34] of the dexterous hand in the camera coordinate frame. $J_{\text{init}}, J_{\text{end}} \in \mathbb{R}^{20}$ correspond to the 20-DoF joint angles of the hand in the pre-grasp and final grasp configurations, respectively.

Hand Coordinate Frames: We define multiple coordinate frames for the hand, including the base frame $\mathcal{F}_{\text{base}}$, the tool center point frame \mathcal{F}_{tcp} , the base frame of each finger \mathcal{F}_{f_i} , and the fingertip plane frame \mathcal{F}_{tip} . The frame \mathcal{F}_{tip} is defined by translating \mathcal{F}_{tcp} along its z -axis such that the sum of vertical distances from all fingertip points $P_i = (x_i, y_i, z_i)$ to the xy -plane of \mathcal{F}_{tip} is minimized. Here, $i = 0, 1, 2, 3, 4$ denote the thumb, index, middle, ring, and little fingers, respectively, as illustrated in Fig. 1(b).

Task Description: Given a scene containing j objects, a single-view point cloud $\mathcal{P} \in \mathbb{R}^{N \times 3}$ is captured by a depth camera. The proposed end-to-end grasp prediction network, DGS-Net, takes \mathcal{P} as input and predicts the dexterous hand's TCP T , hand rotations R , and joint configurations J_{init} and J_{end} for each object. The robot then executes grasping actions sequentially based on the predicted grasp scores, aiming to complete the task of multi-object removal from the scene.

To support this task, we propose a two-stage dataset generation pipeline for constructing training data. In the first stage, a dense set of candidate grasps $\mathcal{G} = \{G_0, G_1, \dots, G_n\}$ is

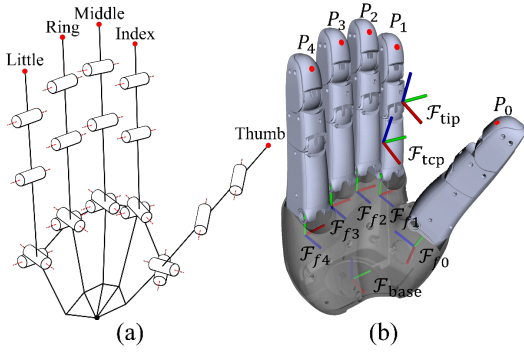


Fig. 1. (a) Joint configuration. (b) Fingertip points and coordinate systems.

generated for each individual object using a fingertip constraint strategy, where n denotes the number of feasible grasp configurations. In the second stage, j objects are randomly placed into a shared scene, and the grasp set \mathcal{G} from the first stage is transformed to the scene to form $\tilde{\mathcal{G}} = \{\mathcal{G}_0, \mathcal{G}_1, \dots, \mathcal{G}_j\}$. We then filter $\tilde{\mathcal{G}}$ based on whether the dexterous hand collides with objects in the scene, resulting in the final scene-level dense grasp set $\mathcal{G}_{\text{scene}}$. In simulation, we render RGB and depth images from multiple viewpoints and generate a set of single-view point clouds $\{\mathcal{P}_k \mid k = 1, 2, 3, \dots\}$, which are paired with $\mathcal{G}_{\text{scene}}$ to construct the training samples $(\mathcal{P}_k, \mathcal{G}_{\text{scene}})$.

IV. GRASPING PREDICTION

In this section, we introduce DGS-Net, an end-to-end network for dexterous grasp prediction. The overall pipeline is illustrated in Fig. 2. Our network adopts Point Transformer V3 (PTv3) [21] as the backbone, leveraging its large receptive field and multi-scale self-attention mechanisms to capture rich global and local point cloud features.

DGS-Net consists of two modules. The first module utilizes PTv3 to extract multi-scale global features from the scene point cloud, and predicts a grasp reference point score as well as the corresponding 6D rotation representation for each point. The second module aggregates local point cloud features and global point cloud features through a self-attention module, and further predicts the grasp offset as well as the pre-grasp and final grasp configurations. The grasp offset is used to compensate for the error between the dexterous hand’s TCP and the grasp reference point in the point cloud caused by point cloud incompleteness or sensor noise. To improve the learning capability of the model, additional intermediate supervision is introduced during training. The second module takes the ground-truth grasp reference point scores and 6D rotations as inputs during training, while during inference, it directly uses the predictions from the first module.

Specifically, our network employs PTv3 to extract multi-scale global features $f \in \mathbb{R}^{N \times C}$ from the scene point cloud $\mathcal{P}_k \in \mathbb{R}^{N \times 3}$, where C denotes the feature dimension. Sparse convolution layers are then applied to predict the grasp reference point scores $G_s \in \mathbb{R}^{N \times 2}$ and the 6D rotation representation $R \in \mathbb{R}^{N \times 6}$ for each point. Based on these, the grasp reference point scores G_s , grasp poses R , and global

point cloud features f are fed into a self-attention encoder followed by multiple sparse convolution layers to predict the pre-grasp joint angles $J_{\text{init}} \in \mathbb{R}^{20}$, the final grasp joint angles $J_{\text{end}} \in \mathbb{R}^{20}$, and the grasp offset $\sigma \in \mathbb{R}^3$. The final TCP of the dexterous hand is computed as $T = P_{G_s} + \sigma$, where $P_{G_s} \in \mathbb{R}^3$ is selected from the input point cloud \mathcal{P}_k by first filtering points with $G_s > 0.7$ and then applying spatial non-maximum suppression (NMS).

We observe that directly regressing high-dimensional joint angles from raw point clouds is challenging due to the weak correlation between point cloud geometry and joint configurations. Therefore, we decompose grasp prediction into two modules: a global understanding module that identifies feasible grasp locations and orientations from holistic scene context, and a grasp refinement module that leverages local geometric features to predict precise hand’s TCP and joint configurations. In addition, our network explicitly learns a grasp offset σ to compensate for point cloud incompleteness and sensor noise, improving grasp accuracy and diversity.

Loss Function:

For grasp reference point prediction, we introduce grasp point semantic labels, where points in our dataset are annotated as grasp reference points, grasp candidate points, or non-graspable points. Since the number of non-graspable points in the point cloud is overwhelmingly larger than that of grasp reference points, the sample distribution is highly imbalanced. Using a standard cross-entropy loss in this case would easily bias the model toward predicting all points as negative. To address this, we treat grasp candidate points as positive samples and apply weighted cross-entropy loss with category-specific weights (grasp reference points: highest weight 2, grasp candidate points: medium weight 1, non-graspable: lowest weight 0.1) where grasp candidate points serve as auxiliary positives to balance sample ratios and form spatially coherent “potentially graspable regions”, thereby enhancing training stability and robustness against sparse annotations. The loss function is defined as follows:

$$\mathcal{L}_{\text{gp}} = -\frac{1}{N} \sum_{i=1}^N \omega_i y_i^{\text{gt}} \log \hat{y}_i \quad (1)$$

Where ω_i denotes the weight for positive or negative samples, y_i^{gt} is the ground-truth label, and \hat{y}_i is the predicted output of the model.

For grasp rotation regression, inspired by the work of Yi Zhou et al. [34], we represent 3D rotations using a 6D vector formed by concatenating two orthogonal 3D vectors. Unlike Euler angles or quaternions, this method is continuously differentiable in Euclidean space, avoiding training instability and performance degradation from rotation space topological discontinuities. In this work, we introduce two loss functions for pose regression: Mean Squared Error (MSE), which measures element-wise errors in the rotation matrix, and Geodesic Rotation Error Loss [35], which captures the minimal angular difference between the predicted and ground-truth rotations. These two losses are combined in a weighted

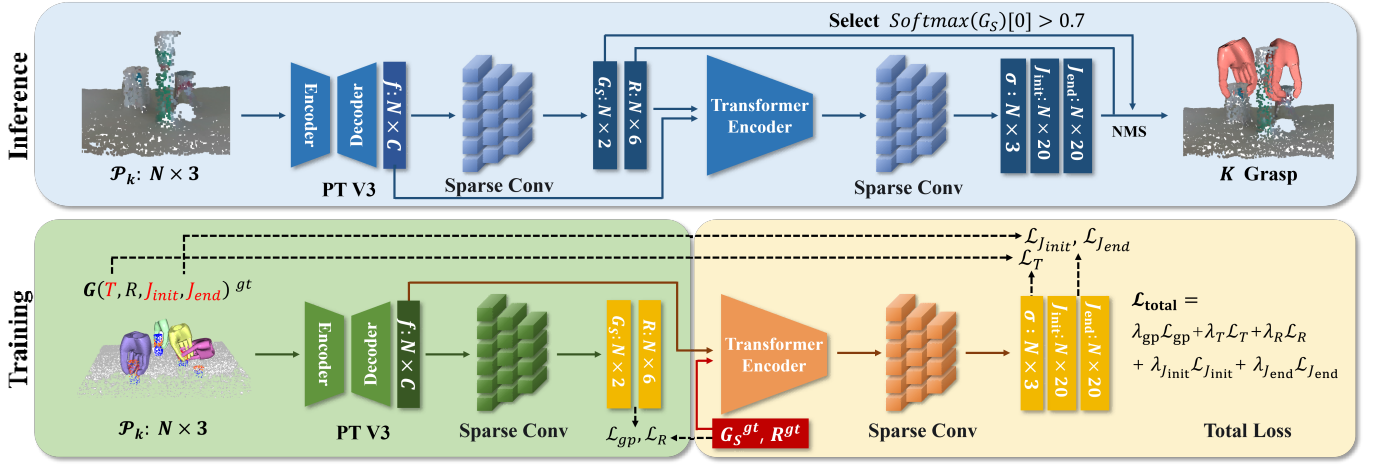


Fig. 2. Overview of DGS-Net. PTv3 extracts multi-scale point cloud features. Module I (green) predicts grasp reference point and 6D rotations; Module II (yellow) generates grasp offsets and joint configurations. During training (bottom), ground-truth grasp reference point and pose labels guide Module I to speed convergence and improve stability. During inference (top), Module II uses Module I predictions, forming an end-to-end pipeline.

manner to balance numerical stability and geometric accuracy.

$$\mathcal{L}_{\text{Mat}} = \frac{1}{N} \sum_{i=1}^N \left\| \hat{R}_i - R_i^{\text{gt}} \right\|_F^2 \quad (2)$$

$$\mathcal{L}_{\text{Geo}} = \frac{1}{N} \sum_{i=1}^N \cos^{-1} \left[0.5 \left(\text{Tr} \left(\hat{R}_i^{\top} R_i^{\text{gt}} \right) - 1 \right) \right] \quad (3)$$

$$\mathcal{L}_R = (1 - \lambda) \mathcal{L}_{\text{Mat}} + \lambda \mathcal{L}_{\text{Geo}} \quad (4)$$

where $\| \cdot \|_F$ denotes the Frobenius norm, \hat{R}_i represents the predicted rotation matrix, R_i^{gt} denotes the ground-truth rotation matrix, $\text{Tr}(\cdot)$ is the trace of a matrix, and λ is the loss weight.

Due to point cloud discreteness and sensor noise, the highest-scoring grasp reference points often deviates from the dexterous hand's TCP. To address this, our network includes an offset prediction branch to regress the displacement between grasp reference points and hand's TCP, combining the top-scoring grasp reference point with the predicted offset to compute the dexterous hand's TCP. We use Relative L1 Loss to maintain sensitivity to small-magnitude offsets.

$$\mathcal{L}_T = \frac{1}{N} \sum_{i=1}^N \frac{|\hat{\sigma}_i - \sigma_i^{\text{gt}}|}{|\sigma_i^{\text{gt}}| + \varepsilon} \quad (5)$$

For the prediction of dexterous hand joint configurations, we directly apply the standard MSE loss to both the pre-grasp and final joint angles, denoted as $\mathcal{L}_{J_{\text{init}}}$ and $\mathcal{L}_{J_{\text{end}}}$, respectively.

Finally, the overall loss are summarized as follows:

$$\mathcal{L}_{\text{total}} = \lambda_{\text{gp}} \mathcal{L}_{\text{gp}} + \lambda_T \mathcal{L}_T + \lambda_R \mathcal{L}_R + \lambda_{J_{\text{init}}} \mathcal{L}_{J_{\text{init}}} + \lambda_{J_{\text{end}}} \mathcal{L}_{J_{\text{end}}} \quad (6)$$

Where λ_* denotes the weights assigned to each loss component.

Note that only points labeled as grasp reference points in the semantic labels are associated with valid grasp annotations, including grasp pose, offset, and joint configurations. Therefore, the rotation loss (\mathcal{L}_R), the offset loss (\mathcal{L}_T), and the joint configuration losses ($\mathcal{L}_{J_{\text{init}}}$ and $\mathcal{L}_{J_{\text{end}}}$) are computed exclusively for grasp reference points.

V. DATASET GENERATION

Grasping involves not only object-gripper interactions but also complex environmental and inter-object influences. To capture these factors and improve robustness for sim-to-real transfer, we adopt a two-stage dataset generation strategy. We collected 307 objects from existing datasets and online sources, each scaled by five scaling factors (0.8, 0.9, 1.0, 1.1, 1.2), and categorized them into five geometric classes: Cuboid, Cylinder, Stick, Sphere, Bowl. All simulations were conducted using PyBullet. [36].

A. Single-Object Grasp Dataset Collection

Single-object grasp data generation aims to construct a dense and diverse set of physically feasible dexterous grasps for each individual object, which serves as the foundation for subsequent scene-level grasp synthesis. Instead of relying on predefined grasp gestures, we systematically explore the grasp space by jointly sampling grasp positions, orientations, and finger participation patterns, enabling broad coverage of potential dexterous grasp configurations while maintaining physical plausibility.

As illustrated in Fig. 3(a), each object is first placed at a predefined pose. The tool center point frame \mathcal{F}_{tcp} of the dexterous hand is randomly placed within the object's bounding box, followed by random rotational perturbations within $[-180^\circ, 180^\circ]$ applied along the X , Y , and Z axes of the TCP frame \mathcal{F}_{tcp} , resulting in diverse grasp poses. To further increase grasp diversity without explicitly predefining hand gestures, we vary the number of participating fingers and consider three configurations: five-finger, two-finger (thumb and index), and three-finger (thumb, index, and middle).

To obtain feasible grasp configurations from the grasp search space, the dexterous hand is first initialized in a fully open configuration. During closure, circular or rectangular constraints are imposed on the fingertip plane (as illustrated in Fig 3(b)) to determine the target positions of each fingertip. These constraints are governed by two parameters: r , which

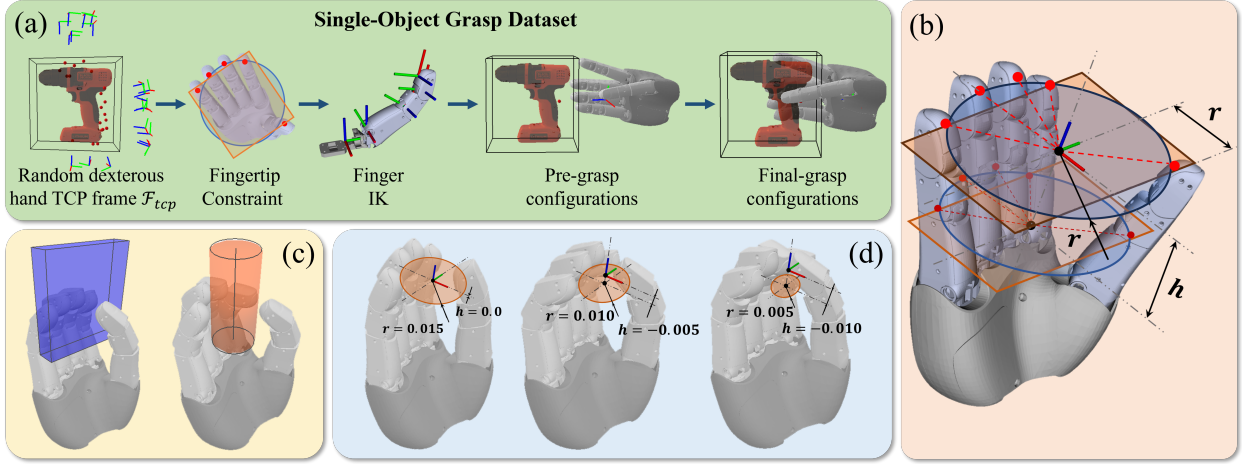


Fig. 3. (a) Single-object grasp data generation pipeline, generating dense grasps for a single object using fingertip point constraints and admittance control. (b) Circular/rectangular fingertip point constraints. (c) Grasps under different fingertip point constraints. (d) Grasp joint configurations under circular constraints with varying parameters r and h .

denotes the radius of the circle or half the width of the rectangle, and h , which represents the distance from the expected positions of the fingertips to the fingertip plane.

Circular constraint:

$$\theta_0 = 15^\circ, \quad \theta_i = 120^\circ + \frac{(i-1)}{4} \times 120^\circ \quad (7a)$$

$$x_i = r \cos(\theta_i) \quad (7b)$$

$$y_i = r \sin(\theta_i) \quad (7c)$$

$$z_i = h + \delta_i \quad (7d)$$

Rectangular constraint:

$$x_0 = 0.8r, \quad x_i = -r \quad (8a)$$

$$y_0 = 0.005, \quad y_i = 0.025(i-2.5) \quad (8b)$$

$$z_i = h + \delta_i \quad (8c)$$

Here, the fingertip point $P_i^{\text{tip}} = (x_i, y_i, z_i)$ is expressed in the fingertip plane frame \mathcal{F}_{tip} , where $i = 0, 1, 2, 3, 4$ denotes the finger index, and δ_i is a finger-specific offset determined by the mechanical structure of the dexterous hand.

The rectangular constraint is suitable for grasping planar objects, while the circular constraint is more appropriate for grasping curved objects such as cylinders and spheres, as illustrated in Fig. 3(c). To generate more diverse grasp samples, we randomly sample the parameters r and h , where different combinations correspond to varying degrees of hand closure (see Fig. 3(d)). This enables the generation of a richer set of grasp closure configurations.

By applying the target constraints, the desired fingertip position for each finger P_i^{tip} is obtained. This point is then transformed into the local coordinate frame of the corresponding finger \mathcal{F}_{f_i} using the transformation matrix $\mathbf{T}_{\text{tip}}^{f_i}$, resulting in the local position: $P_i^{f_i} = \mathbf{T}_{\text{tip}}^{f_i} P_i^{\text{tip}}$. The desired joint angles for each finger, denoted as $\Theta_i = (\theta_{i1}, \theta_{i2}, \theta_{i3}, \theta_{i4})$, are computed via inverse kinematics, where θ_{i3} and θ_{i4} are kinematically coupled. During grasp execution, the fingers are actuated using admittance control.

During the admittance control process, the finger is modeled as a mass-damper-spring system, and its motion under external forces is simulated through numerical integration. A relatively low stiffness coefficient K is selected to allow the finger to closely conform to the object surface. The joint angles obtained at the end of simulation are recorded as the dexterous hand's final grasp configuration J_{end} .

The pre-grasp gesture J_{init} is derived by scaling the final grasp joint angles J_{end} , with the scaling factors determined empirically. Considering the significant influence of the finger base's yaw and pitch joints on the overall finger posture, a larger scaling factor (0.6) is applied to the pitch joints, while the yaw joints are kept identical to the final grasp configuration (i.e., a scaling factor of 1.0) to preserve the primary grasp posture. For the coupled distal joints, a smaller scaling factor (0.2) is adopted to prevent excessive fingertip closure and premature contact with the object during the approach phase. Here, the pitch and yaw joints refer to rotations about the local x - and z -axes, respectively.

$$J_{\text{init}} = \{\theta_{i1}, 0.6\theta_{i2}, 0.2\theta_{i3}, 0.2\theta_{i4} \mid \theta_{ij} \in J_{\text{end}}\} \quad (9)$$

For two-finger and three-finger grasps, the fingers not involved in the grasp retain the same joint configuration in the pre-grasp gesture as in the final grasp gesture. During data collection, the dexterous hand approaches the target object from a distance of 0.1 meters using J_{init} . If any collision occurs with the target or surrounding objects during this approach, the grasp attempt is considered a failure. Once the grasp pose is reached, the fingers are closed to the final joint configuration J_{end} under admittance control, with control parameters chosen to resemble those of real-world dexterous hand executions. A grasp is considered successful if the fingers can effectively envelop the object and maintain stable contact after applying gravity forces along all six axes for 100 simulation steps.

B. Scene-Level Grasp Dataset Collection

The scene-level grasp dataset is constructed to bridge the gap between isolated object grasp synthesis and realistic

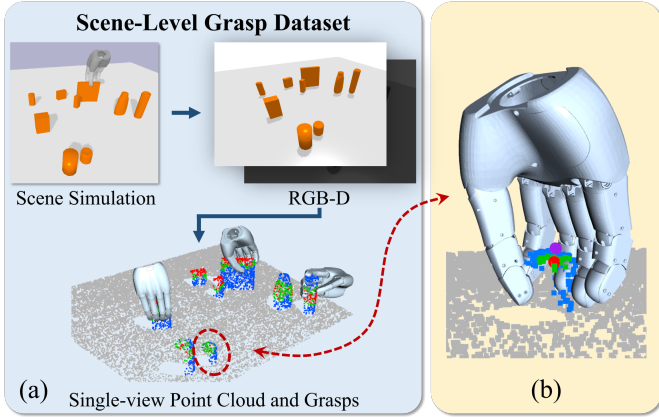


Fig. 4. (a) Scene-level grasp data generation pipeline. (b) Grasp labels on point cloud: blue represents object point clouds; purple denotes the dexterous hand’s TCP T ; Red indicates grasp reference points, which are the points in the object point cloud closest to the hand’s TCP; green denotes grasp candidate points in the neighborhood of each grasp reference point; gray point clouds correspond to the tabletop.

multi-object environments, enabling the model to learn grasp feasibility under object-object interactions and environmental constraints. To achieve this, We leverage the single-object grasp sets generated in the first stage and transfer them to multi-object scenes, followed by feasibility validation, which ensures both efficiency and physical consistency.

As shown in Fig. 4(a), a scene is constructed by randomly sampling 5-15 objects from the first-stage dataset and allowing them to fall under gravity into a stable configuration. The individual-object grasp sets $\mathcal{G} = \{G_0, G_1, \dots, G_i\}$ are then mapped to the scene, yielding candidate grasps $\tilde{\mathcal{G}} = \{\mathcal{G}_0, \mathcal{G}_1, \dots, \mathcal{G}_j\}$. Each grasp is validated for collisions, and only those with collision-free approaches are retained as the final scene-level grasp set $\mathcal{G}_{\text{scene}}$. This allows the network to implicitly learn environmental constraints.

Each scene is captured from 256 uniformly sampled viewpoints over a 1-meter-radius hemisphere (elevation: 22.5°-67.5°, azimuth: 0°-360°). For each view, we record the grasp configurations, RGB-D images, segmentation masks, camera extrinsics, and object occlusion relationships.

Notably, the dexterous hand’s TCPs generated in Stage 1 are randomly placed within object bounding boxes and do not directly correspond to discrete points in the scene-level point cloud. To generate semantic labels for grasp supervision, we first downsample the scene point cloud and construct a KD-tree for efficient nearest-neighbor search. Each hand’s TCP is then associated with its nearest point in the downsampled point cloud, which is designated as the grasp reference point. In addition, the 20 nearest neighboring points surrounding each grasp reference point are labeled as grasp candidate points, representing potential grasp regions (see Fig. 4(b)). The semantic labels are assigned in a mutually exclusive manner, where grasp reference points take precedence over grasp candidate points in cases of overlap.

Due to single-view point cloud incompleteness, a discrepancy may exist between the dexterous hand’s TCP and the corresponding grasp reference point. To address this, we record

the grasp offset for each instance as additional supervision, using it as auxiliary supervision to correct geometric errors and improve robustness in occluded or unseen regions.

The final training labels consist of:

- Grasp point semantic labels for point clouds, which could be “grasp reference point”, “grasp candidate point”, or “non-graspable”;
- Grasp offset vectors;
- Dexterous hand grasp poses in the camera frame, along with pre-grasp and final joint configurations.

C. Dataset Overview

Our dataset contains 307 objects spanning five categories (Cuboid, Sphere, Cylinder, Stick, Bowl). The distribution of these object categories, and the grasp distribution of different hand gestures across each category, is presented in Table I.

TABLE I
OBJECT AND GRASP DATA DISTRIBUTION

| | Object Count | Grasps(%) | | |
|----------|--------------|-----------|---------|---------|
| | | 5finger | 3finger | 2finger |
| Cuboid | 116 | 46.652 | 0 | 0 |
| Cylinder | 69 | 23.147 | 0 | 0 |
| Stick | 72 | 18.031 | 3.366 | 0.231 |
| Sphere | 26 | 4.123 | 2.596 | 0 |
| Bowl | 24 | 1.178 | 0.231 | 0.034 |

Our dataset contains over 60k RGB-D images from 240 multi-object scenes, each with 5-15 randomly selected objects, captured from 256 viewpoints per scene, yielding more than 350k valid grasp instances. Each sample includes the scene point cloud, grasp point semantic labels, dexterous hand grasp poses, pre-grasp and final joint configurations, occlusion information, and segmentation masks. In contrast to most existing datasets that provide only grasp poses and final joint configurations, our dataset additionally includes pre-grasp joint configurations, grasp offsets, grasp point semantic labels, and scene occlusion information, which facilitate precise grasp prediction and improve robustness in multi-object and partially observed scenes.

VI. EXPERIMENTS

In this section, we first present the experimental setup, including evaluation metrics and implementation details. Subsequently, we validate the proposed method on both simulation and real robotic platforms. Experimental results demonstrate that, compared to existing baseline methods, our model can generate more robust grasp candidates, achieving improved grasp success rates and scene clearance rates with lower penetration.

A. Experimental Setup

Evaluation Metrics: To assess the performance of our proposed method, we adopt three quantitative metrics commonly used in previous works [28], [33]:

- Grasp Success Rate (SR) (unit: %): The percentage of successful grasps relative to the attempt number.

- Scene Clearance Rate (CR) (unit: %): The percentage of objects successfully grasped in a scene to the total number of objects present in a multi-object scene.
- Penetration Depth (PD) (unit: mm): The maximum intersection distance between the hand and object for each grasp.
- Penetration Volume (PV) (unit: mm^3): The volume of mutual interpenetration between the hand and object for each grasp.
- Diversity (D) (unit: %): The proportion of total variance explained by the first principal component in PCA, computed as the ratio of the first eigenvalue to the sum of all eigenvalues. PCA is performed on data points that include hand’s TCP T , rotation R (in the axis-angle representation), and joint angles J_{init} , J_{end} .
- Time Cost (TC) (unit: s): The average inference time required for a single grasp prediction.

Implementation Details: Our network takes a scene point cloud as input, from which 20,000 points are sampled. The model is trained using the Adam optimizer with a learning rate of 0.001 and a batch size of 10 for a total of 40 epochs. Training is conducted on a single NVIDIA RTX 4090 GPU, with an overall training time of approximately 27 hours.

B. Simulation Experiments

Experiments are conducted in a simulator following this protocol: 240 novel multi-object test scenes are constructed, each containing 10 randomly arranged objects within a 0.6×0.6 m workspace. For each scene, single-view point clouds are sampled from random viewpoints on a hemisphere of 1 m radius centered on the scene. After each model prediction, the grasp with the highest predicted grasp score is executed. The dexterous hand first approaches the target object in the pre-grasp configuration and then executes the final grasp in the final grasp configuration. A grasp is considered successful if the object is lifted at least 10 cm. After each grasp attempt, regardless of success or failure, the scene point cloud is re-captured and re-evaluated. Successfully grasped objects are removed from the scene, while objects that fail three grasping attempts are also removed. This iterative process continues until no graspable objects remain in the scene.

Ablation Experiments: To evaluate the effectiveness of the proposed pre-grasp configuration and grasp offset, we conduct the ablation experiments presented in Table II. All experiments are performed using DGS-Net trained with both the adaptive pre-grasp configuration and the grasp offset. In the without pre-grasp setting, the network-predicted pre-grasp configurations are replaced with a fixed open-hand configuration ($J_{init} = \{\theta_{ij} = 0\}$). In the without offset setting, the network-predicted grasp offset vectors are discarded and uniformly set to zero. In the full setting, both the pre-grasp configuration and grasp offset vectors predicted by the network are applied.

Experimental results confirm that both pre-grasp configurations and grasp offsets improve grasping success. Fixed pre-grasp configurations lead to higher collision rates in multi-object scene. In contrast, our adaptive pre-grasps facilitate

more coordinated five-finger contact, preventing object slip-page caused by sequential finger contact. The grasp offset further compensates for position deviations caused by occlusions and sensor noise, thereby improving grasp stability.

Grasp Efficiency: We further evaluate DGS-Net on the dataset used by the baseline method HGC-Net [28] dataset. As shown in Table III, our method achieves higher grasp success rates and scene clearance rates, indicating strong generalization capability. Although the runtime is slightly longer (0.45s vs. 0.25s for HGC-Net), it remains sufficient for scene-level grasping tasks, where prediction speed is not the primary bottleneck. Compared with the state-of-the-art method DexGraspNet 2.0 [29] (abbreviated as DGN 2.0 in the table), our approach achieves comparable performance using a smaller-scale dataset, with slightly higher grasp success rates but slightly lower scene clearance rates. This indicates that our network learns grasp-relevant representations more efficiently and makes more effective use of training data. In addition, to ensure comparability with real-world grasping experiments, we include an additional set of simulation experiments in which 4-6 objects are randomly placed within a 0.4×0.8 m workspace, consistent with the real-world experimental setup.

We further benchmark our method against a pipeline consisting of object segmentation, shape completion, and single-object grasp prediction (Multi-FinGAN [27], DVGG [10], and Humt et al. [14]). In comparison, our method is significantly faster, while these pipelines achieve slightly higher grasp success rates. It is worth emphasizing that our results are obtained in more challenging multi-object scenes. Therefore, these results indicate our approach robust performance in challenging multi-object scenes.

Grasp Quality: We further evaluate grasp quality in simulation using penetration depth, penetration volume, and grasp diversity, as reported in Table IV. Compared with baseline methods, our approach achieves notably smaller penetration depth and penetration volume, indicating more accurate hand-object alignment and improved physical consistency during grasp execution. In addition, the variance of both PD and PV is significantly reduced, suggesting that the predicted grasps are not only less penetrative but also more stable and consistent across different scenes.

In terms of grasp diversity, our method performs slightly worse than DexGraspNet 2.0 [29] and Dexonomy [33], which is trained on a substantially larger-scale dataset. This result is expected, as larger datasets tend to promote broader grasp distribution. Nevertheless, our method maintains competitive diversity while achieving superior penetration-related metrics, even when trained on a smaller dataset. This indicates strong representation learning capability, efficient utilization of training data, and improved consistency between the learned grasp

TABLE II
ABLATION STUDIES IN SIMULATION

| Pre-grasp | offset | SR(%) | | | | | | CR(%) |
|-----------|--------|--------------|--------------|--------------|--------------|--------------|--------------|--------------|
| | | Cuboid | Cylinder | Stick | Sphere | Bowl | Total | |
| ✗ | ✓ | 71.79 | 72.24 | 68.72 | 32.07 | 65.21 | 69.83 | 80.58 |
| ✓ | ✗ | 74.67 | 75.92 | 65.28 | 36.17 | 64.64 | 71.10 | 82.07 |
| ✓ | ✓ | 77.49 | 79.25 | 72.42 | 42.42 | 74.51 | 74.81 | 84.73 |

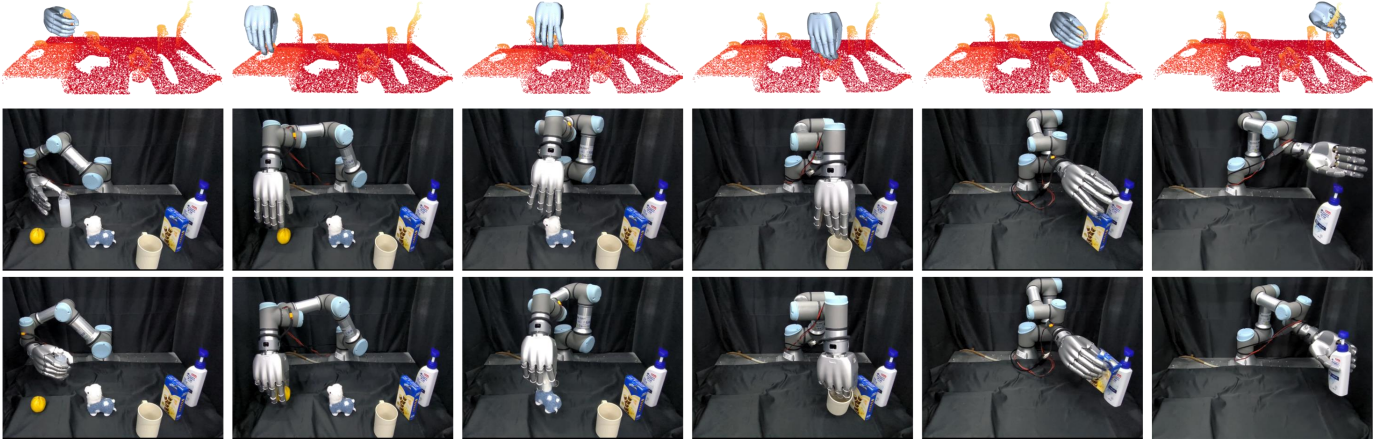


Fig. 5. Real-world execution pipeline: (top) model prediction, (middle) pre-grasp configuration, and (bottom) final grasping execution.

TABLE III
GRASP EFFICIENCY EXPERIMENT RESULTS

| | Objects/Scene | Dataset | SR(%) | CR(%) | Time Cost(s) |
|-------------------|---------------|--------------------------|--------------|--------------|--------------|
| HGC-Net [28] | 10 | HGC-Net | 71.9 | 78.8 | 0.25 |
| DGS-Net | 10 | | 73.07 | 81.13 | 0.45 |
| DGS-Net | 10 | Ours (Include YCB) | 74.81 | 84.73 | 0.45 |
| DGN 2.0 [29] | 10 | | 73.59 | 83.87 | 0.5 |
| DGS-Net | 4-6 | | 88.63 | 87.06 | 0.45 |
| Multi-FinGAN [27] | 1 | YCB | 60 | - | 7.4 |
| DVGG [10] | 1 | | 72.4 | - | 0.9 |
| Humt et al. [14] | 1 | | 95.2 | - | 1.1 |

TABLE V
REAL-WORLD EXPERIMENTAL RESULTS

| | Ours | HGC-Net [28] | Kiatos et al. [26] | Graspit! |
|-------|--------------|--------------|--------------------|----------|
| SR(%) | 78.98 | 66.7 | 74.0 | 58.5 |
| CR(%) | 86.86 | 75.0 | 75.0 | 54.3 |

C. Robot Experiments

To evaluate the sim-to-real generalization of our method, we deployed a real-world grasping platform consisting of a DexHand Pro mounted on a UR3 robotic arm (Fig. 6(a)). Scene point clouds were captured by a global RealSense D455 depth camera, and arm motions were planned with MoveIt!. For transparent objects, depth estimation was performed using FoundationStereo [37]. In all trials, the grasp pose with the highest network-predicted score within the robot workspace was selected, along with its associated offset, pre-grasp, and final grasp configurations. The real-world experiments followed the same protocol as the simulation, with two key differences: (1) each scene contained 4-6 real objects randomly arranged within a 0.4×0.8 m workspace, and (2) the object set consisted of 29 novel items (Fig. 6(b)). Across 25 distinct scenes, we performed a total of 138 grasp attempts.

As shown in Table V, our method achieves a grasp success rate (SR) of 78.98% and a clearance rate (CR) of 86.86% in real-world environments, outperforming all baseline methods. Without any fine-tuning on real-world data,

our model maintains high performance due to the following key design features:

- 1) A modular network architecture that first captures global scene context to predict grasp regions, followed by fine-grained reasoning over local geometric features to generate precise joint configurations;
- 2) The introduction of pre-grasp configuration, which align better with real-world execution and help avoid collisions during approach, thereby enhancing grasp stability and feasibility;
- 3) Explicit modeling of grasp offsets, which compensates for position deviations caused by occlusions and sensor noise in sparse point clouds, improving generalization



Fig. 6. Real-world experimental setup: (a) UR3 with a DexHand Pro and an overhead depth camera capturing scene point clouds; objects placed in a 0.4×0.8 m workspace. (b) The 29 real-world test objects (unseen during training).

distributions and physical constraints. Overall, these results demonstrate that DGS-Net can generate physically plausible and robust dexterous grasps in multi-object scenes.

TABLE IV
GRASP QUALITY EXPERIMENT RESULTS

| | PD(mm) ↓ Mean ± Variance | PV(mm ³) ↓ Mean ± Variance | D(%) ↓ |
|---------------|-----------------------------|---|--------------|
| HGC-Net [28] | 12.93 ± 5.28 | 13970 ± 13206 | 51.23 |
| GraspTTA [12] | 8.21 ± 4.63 | 2647.70 ± 1744.08 | 48.80 |
| DVGG [10] | 4.10 ± - | 3800 ± - | - |
| Dexonomy [33] | 8.28 ± 7.76 | 7314.02 ± 10163.44 | 25.70 |
| DGN 2.0 [29] | 0.594 ± 7.13 | 1452.24 ± 3056.10 | 27.14 |
| DGS-Net | 0.375 ± 4.53 | 559.45 ± 1262.10 | 35.18 |

in unstructured environments.

VII. CONCLUSION

This study addresses multi-fingered dexterous grasping in multi-object scene by constructing a high-quality dataset from single-view point clouds, and proposing an end-to-end grasp prediction network that directly infers grasp positions, grasp poses, and dexterous hand joint configurations from incomplete observations. By explicitly modeling grasp offsets and pre-grasp configurations, the proposed method effectively compensates for projection errors and occlusions, reducing unnecessary hand-object collisions that may lead to grasp failures, and leading to more accurate hand-object alignment. These properties make the proposed approach particularly suitable for safety-critical and unstructured application scenarios, such as intelligent manufacturing and chemical industry environments. Extensive simulation and real-world experiments demonstrate that DGS-Net achieves high grasp success and scene clearance rates, while consistently producing grasps with lower penetration, validating its robustness and generalization capability under partial observations.

Furthermore, We observe that the robotic arm plays a crucial role in grasping outcomes, yet most methods focus on hand-object interactions while overlooking kinematic constraints and motion planning. Future work will thus aim to: (1) couple grasp synthesis with arm trajectory optimization to improve feasibility and success, (2) adapt the approach to various dexterous hands, (3) enable object- and part-specific grasping via semantic segmentation or detection, and (4) expand the dataset, especially for two- and three-finger grasps.

REFERENCES

- [1] R. Newbury, M. Gu, L. Chumbley, A. Mousavian, C. Eppner, J. Leitner, J. Bohg, A. Morales, T. Asfour, D. Kragic, D. Fox, and A. Coşgun, "Deep Learning Approaches to Grasp Synthesis: A Review," *IEEE Transactions on Robotics*, vol. 39, no. 5, pp. 3994–4015, Oct. 2023.
- [2] J. Bohg, A. Morales, T. Asfour, and D. Kragic, "Data-Driven Grasp Synthesis—A Survey," *IEEE Transactions on Robotics*, vol. 30, no. 2, pp. 289–309, Apr. 2014.
- [3] A. Billard and D. Kragic, "Trends and challenges in robot manipulation," *Science*, Jun. 2019.
- [4] A. Miller and P. Allen, "Grasplit! A versatile simulator for robotic grasping," *IEEE Robotics & Automation Magazine*, vol. 11, no. 4, pp. 110–122, Dec. 2004.
- [5] H. Dai, A. Majumdar, and R. Tedrake, "Synthesis and Optimization of Force Closure Grasps via Sequential Semidefinite Programming," in *Robotics Research: Volume 1*, A. Bicchi and W. Burgard, Eds. Cham: Springer International Publishing, 2018, pp. 285–305.
- [6] N. Bergström, J. Bohg, and D. Kragic, "Integration of Visual Cues for Robotic Grasping," in *Computer Vision Systems*, M. Fritz, B. Schiele, and J. H. Piater, Eds. Berlin, Heidelberg: Springer, 2009, pp. 245–254.
- [7] V.-D. Nguyen, "Constructing Force-Closure Grasps," *The International Journal of Robotics Research*, Jun. 1988.
- [8] S. Thalhammer, D. Bauer, P. Hönig, J.-B. Weibel, J. García-Rodríguez, and M. Vincze, "Challenges for Monocular 6-D Object Pose Estimation in Robotics," *IEEE Transactions on Robotics*, vol. 40, pp. 4065–4084, 2024.
- [9] Y. Huang, D. Fan, H. Duan, D. Yan, W. Qi, J. Sun, Q. Liu, and P. Wang, "Human-like dexterous manipulation for anthropomorphic five-fingered hands: A review," *Biomimetic Intelligence and Robotics*, vol. 5, no. 1, p. 100212, Mar. 2025.
- [10] W. Wei, D. Li, P. Wang, Y. Li, W. Li, Y. Luo, and J. Zhong, "DVGG: Deep Variational Grasp Generation for Dextrous Manipulation," *IEEE Robotics and Automation Letters*, vol. 7, no. 2, pp. 1659–1666, Apr. 2022.
- [11] V. Mayer, Q. Feng, J. Deng, Y. Shi, Z. Chen, and A. Knoll, "FFHNet: Generating Multi-Fingered Robotic Grasps for Unknown Objects in Real-time," in *2022 International Conference on Robotics and Automation (ICRA)*. Philadelphia, PA, USA: IEEE, May 2022, pp. 762–769.
- [12] H. Jiang, S. Liu, J. Wang, and X. Wang, "Hand-object contact consistency reasoning for human grasps generation," Apr. 2021.
- [13] A. Kirillov, E. Mintun, N. Ravi, H. Mao, C. Rolland, L. Gustafson, T. Xiao, S. Whitehead, A. C. Berg, W.-Y. Lo, P. Dollar, and R. Girshick, "Segment anything," in *Proceedings of the IEEE/CVF International Conference on Computer Vision*, 2023, pp. 4015–4026.
- [14] M. Humt, D. Winkelbauer, U. Hillenbrand, and B. Bäuml, "Combining Shape Completion and Grasp Prediction for Fast and Versatile Grasping with a Multi-Fingered Hand," in *2023 IEEE-RAS 22nd International Conference on Humanoid Robots (Humanoids)*. Austin, TX, USA: IEEE, Dec. 2023, pp. 1–8.
- [15] A. Boulch and R. Marlet, "POCO: Point Convolution for Surface Reconstruction," in *Proceedings of the IEEE/CVF Conference on Computer Vision and Pattern Recognition*, 2022, pp. 6302–6314.
- [16] H.-S. Fang, C. Wang, M. Gou, and C. Lu, "GraspNet-1Billion: A Large-Scale Benchmark for General Object Grasping," in *Proceedings of the IEEE/CVF Conference on Computer Vision and Pattern Recognition*, 2020, pp. 11 444–11 453.
- [17] S. Back, J. Lee, K. Kim, H. Rho, G. Lee, R. Kang, S. Lee, S. Noh, Y. Lee, T. Lee, and K. Lee, "GraspClutter6D: A Large-scale Real-world Dataset for Robust Perception and Grasping in Cluttered Scenes," Apr. 2025.
- [18] M. Liu, Z. Pan, K. Xu, K. Ganguly, and D. Manocha, "Deep Differentiable Grasp Planner for High-DOF Grippers," Jul. 2020.
- [19] R. Wang, J. Zhang, J. Chen, Y. Xu, P. Li, T. Liu, and H. Wang, "DexGraspNet: A Large-Scale Robotic Dexterous Grasp Dataset for General Objects Based on Simulation," in *2023 IEEE International Conference on Robotics and Automation (ICRA)*. London, United Kingdom: IEEE, May 2023, pp. 11 359–11 366.
- [20] K. Kleiberger, R. Bormann, W. Kraus, and M. F. Huber, "A Survey on Learning-Based Robotic Grasping," *Current Robotics Reports*, vol. 1, no. 4, pp. 239–249, Dec. 2020.
- [21] X. Wu, L. Jiang, P.-S. Wang, Z. Liu, X. Liu, Y. Qiao, W. Ouyang, T. He, and H. Zhao, "Point Transformer V3: Simpler Faster Stronger," in *Proceedings of the IEEE/CVF Conference on Computer Vision and Pattern Recognition*, 2024, pp. 4840–4851.
- [22] M. Breyer, J. J. Chung, L. Ott, R. Siegwart, and J. Nieto, "Volumetric Grasping Network: Real-time 6 DOF Grasp Detection in Clutter," in *Proceedings of the 2020 Conference on Robot Learning*. PMLR, Oct. 2021, pp. 1602–1611.
- [23] H.-S. Fang, C. Wang, H. Fang, M. Gou, J. Liu, H. Yan, W. Liu, Y. Xie, and C. Lu, "AnyGrasp: Robust and Efficient Grasp Perception in Spatial and Temporal Domains," *IEEE Transactions on Robotics*, vol. 39, no. 5, pp. 3929–3945, Oct. 2023.
- [24] H. Liu, K. Wu, P. Meusel, N. Seitz, G. Hirzinger, M. Jin, Y. Liu, S. Fan, T. Lan, and Z. Chen, "Multisensory five-finger dexterous hand: The DLR/HIT Hand II," in *2008 IEEE/RSJ International Conference on Intelligent Robots and Systems*, Sep. 2008, pp. 3692–3697.
- [25] "Shadow Dexterous Hand Series - Research and Development Tool," <https://shadowrobot.com/dexterous-hand-series/>, Sep. 2023.
- [26] M. Kiatos, S. Malassiotis, and I. Sarantopoulos, "A Geometric Approach for Grasping Unknown Objects With Multifingered Hands," *IEEE Transactions on Robotics*, vol. 37, no. 3, pp. 735–746, Jun. 2021.
- [27] J. Lundell, E. Corona, T. Nguyen Le, F. Verdoja, P. Weinzaepfel, G. Rogez, F. Moreno-Noguer, and V. Kyriki, "Multi-FinGAN: Generative Coarse-To-Fine Sampling of Multi-Finger Grasps," in *2021 IEEE International Conference on Robotics and Automation (ICRA)*, May 2021, pp. 4495–4501.
- [28] Y. Li, W. Wei, D. Li, P. Wang, W. Li, and J. Zhong, "HGC-Net: Deep Anthropomorphic Hand Grasping in Clutter," in *2022 International Conference on Robotics and Automation (ICRA)*. Philadelphia, PA, USA: IEEE, May 2022, pp. 714–720.
- [29] J. Zhang, H. Liu, D. Li, X. Yu, H. Geng, Y. Ding, J. Chen, and H. Wang, "DexGraspNet 2.0: Learning Generative Dexterous Grasping in Large-scale Synthetic Cluttered Scenes," in *8th Annual Conference on Robot Learning*, Sep. 2024.
- [30] Y.-W. Chao, W. Yang, Y. Xiang, P. Molchanov, A. Handa, J. Tremblay, Y. S. Narang, K. Van Wyk, U. Iqbal, S. Birchfield, J. Kautz, and D. Fox, "DexYCB: A Benchmark for Capturing Hand Grasping of Objects," in *Proceedings of the IEEE/CVF Conference on Computer Vision and Pattern Recognition*, 2021, pp. 9044–9053.
- [31] S. Hampali, M. Rad, M. Oberweger, and V. Lepetit, "HONnotate: A Method for 3D Annotation of Hand and Object Poses," in *Proceedings of*

- the IEEE/CVF Conference on Computer Vision and Pattern Recognition*, 2020, pp. 3196–3206.
- [32] Y. Liu, Y. Yang, Y. Wang, X. Wu, J. Wang, Y. Yao, S. Schwertfeger, S. Yang, W. Wang, J. Yu, X. He, and Y. Ma, “RealDex: Towards Human-like Grasping for Robotic Dexterous Hand,” in *Proceedings of the Thirty-Third International Joint Conference on Artificial Intelligence*, Aug. 2024, pp. 6859–6867.
 - [33] J. Chen, Y. Ke, L. Peng, and H. Wang, “Dexonomy: Synthesizing All Dexterous Grasp Types in a Grasp Taxonomy,” 2025.
 - [34] Y. Zhou, C. Barnes, J. Lu, J. Yang, and H. Li, “On the Continuity of Rotation Representations in Neural Networks,” in *Proceedings of the IEEE/CVF Conference on Computer Vision and Pattern Recognition*, 2019, pp. 5745–5753.
 - [35] S. S. Mohseni Salehi, S. Khan, D. Erdogmus, and A. Gholipour, “Real-Time Deep Pose Estimation With Geodesic Loss for Image-to-Template Rigid Registration,” *IEEE Transactions on Medical Imaging*, vol. 38, no. 2, pp. 470–481, Feb. 2019.
 - [36] E. Coumans, “Bullet physics simulation,” in *ACM SIGGRAPH 2015 Courses*. Los Angeles California: ACM, Jul. 2015, p. 1.
 - [37] B. Wen, M. Trepte, J. Aribido, J. Kautz, O. Gallo, and S. Birchfield, “FoundationStereo: Zero-Shot Stereo Matching,” Apr. 2025.